JOURNAL OF GEOPHYSICAL RESEARCH, VOL. 98, NO. A10, PAGES 17,235–17,249, OCTOBER 1, 1993

A Global Magnetohydrodynamic Simulation of the Magnetosphere When the Interplanetary Magnetic Field is Southward: The Onset of Magnetotail Reconnection

RAYMOND J. WALKER

Institute of Geophysics and Planetary Physics, University of California, Los Angeles

TATSUKI OGINO

Solar Terrestrial Environment Laboratory, Nagoya University, Toyokawa, Japan

JOACHIM RAEDER AND MAHA ASHOUR-ABDALLA[1]

Institute of Geophysics and Planetary Physics, University of California, Los Angeles

We have used a new high-resolution global magnetohydrodynamic simulation model to investigate the onset of reconnection in the magnetotail during intervals with southward interplanetary magnetic field (IMF). After the southward IMF reaches the dayside magnetopause reconnection begins and magnetic flux is convected into the tail lobes. After about 35 min, reconnection begins within the plasma sheet near midnight at $x = -14R_E$. Later the x line moves toward dawn and dusk. The reconnection occurs just tailward of the region where the tail attaches onto the dipole-dominated inner magnetosphere. The simulation shows that prior to the onset of reconnection, the Poynting flux is concentrated in this region. The time required for the start of reconnection depends on the component of the magnetic field normal to the equator (B_z). Reconnection occurs only after the B_z component has been reduced sufficiently for the tearing mode to grow. Later, when all the plasma sheet field lines have reconnected, a plasmoid moves down the tail.

1. INTRODUCTION

It has long been recognized that the interplanetary magnetic field (IMF) orientation controls magnetospheric dynamics [see *McPherron*, 1990, for a recent review]. Magnetospheric substorms are associated with a southward IMF, and most models of substorm dynamics start with dayside reconnection. The most frequently discussed model is the near-earth neutral-line model. However, this model is not universally accepted. Other models include the driven model [*Akasofu*, 1981*a*, *b*, the boundary layer dynamics model [*Rostoker and Eastman*, 1987], the thermal catastrophe model [*Smith et al.*, 1986; *Goertz and Smith*, 1989], and the near-earth tail current disruption model [*Lui et al.*, 1991]. The models differ most in their dependence on the physics in the near-earth $x > -40R_E$ part of the magnetotail.

In the near-earth neutral-line model the onset of dayside merging is not immediately followed by an increase in reconnection at the distant neutral line in the magnetotail. Instead, flux accumulates in the tail lobes. This leads to a distortion of the magnetosphere in which the tail current sheet moves inward and the current increases while the plasma sheet thins. Tearing-mode reconnection then begins in a localized part of the plasma sheet on closed field lines, forming an x-type neutral line and an o-type neutral line. The expansion phase of the substorm begins when all of the closed plasma sheet field lines have reconnected and reconnection starts on open tail lobe field lines. This is thought to occur explosively. The tension on the lobe magnetic field lines which drape over the o-line pull it tailward.

The near-earth tail current disruption model [*Lui et al.*, 1991] is a variant on the near-earth neutral-line model. In this model the substorm expansion phase corresponds to a disruption of the inner edge of the cross-tail current. The near-earth neutral line and reconnection occur as consequences of the current disruption and after the start of the substorm expansion phase. It has long been known that strong taillike magnetic field distortions and energetic particle dropouts occur at synchronous orbit during the growth phase of the substorm and that rapid field dipolarization and dispersionless particle injections occur at break up [*Kokubun and McPherron*, 1981; *Nagai*, 1984; *DeForest and McIlwain*, 1971; *Baker*, 1984]. Using AMPTE-CCE observations, *Takahashi et al.* [1987] reported that breakup was associated with extremely violent magnetic field fluctuations at $8.1R_E$ which preceded the dipolarization. *Lopez et al.* [1988*a*, *b*], have studied substorm-related magnetic reconfiguration events and found that substorm onset frequently occurs tailward of synchronous orbit but earthward of the apogee of the AMPTE-CCE satellite at $8.8R_E$. They interpreted their observations to indicate the disruption of the near-earth current sheet. Both the synchronous orbit data [*Kaufmann*, 1987] and plasma sheet observations [*Mitchell et al.*, 1990; *Sergeev et al.*, 1990] show that during the growth phase, the near-earth tail current sheet becomes very thin and penetrates into the inner parts of the magnetosphere.

There is no consensus about the location of the reconnection. Many early investigators provided us with evidence that reconnection occurs for $x > -20R_E$ and may occur as close as $x = -10R_E$ [*McPherron et al.*, 1973; *Russell and McPherron*,

[1]Also at Department of Physics, University of California, Los Angeles.

Paper number 93JA01321.
0148-0227/93/93JA-01321$05.00

1973; *Hones et al.*, 1973; *Nishida and Nagayama*, 1973]. *McPherron* [1990] notes that the extremely well documented CDAW-6 (Coordinated Data Analysis Workshop) substorm onsets occurred at $x = -13R_E$. On the other hand, *Huang and Frank* [1986], *Cattell and Mozer*, [1984] (who used ISEE observations), and *Baumjohann et al.* [1989] (who used AMPTE-IRM data) argue that the neutral line usually forms for $x < -20R_E$. In the distant tail ($x < -75R_E$), observations indicate that the magnetic o-regions (plasmoids) are observed for most substorms [*Hones et al.*, 1984; *Slavin et al.*, 1984, 1992]. Finally, a southward IMF does not always lead to reconnection and a full substorm. *Pytte et al.* [1978] and *Sergeev and Lennartsson* [1988] found evidence for periods of enhanced time-dependent convection following a southward turning of the IMF but without evidence of a substorm onset.

Auroral observations support the idea that substorms begin somewhere in the near-earth tail. They indicate that the substorm expansion phase begins with the sudden brightening of the equatorward arc system, which had drifted to lower latitudes during the growth phase [*Sheppard and Murphree*, 1991]. These equatorward arcs are thought to map to the region of maximum cross-tail current located in the near-earth plasma sheet [*Elphinstone et al.*, 1991]. The expansion phase proceeds with the poleward motion of the midnight aurora and the development of one or more westward surges [*Akasofu et al.*, 1965, 1966; *Craven and Frank*, 1987]; both the midnight aurora and the surges move poleward until they reach the most poleward arc.

A number of theoretical studies have investigated magnetospheric convection and the onset of reconnection. *Erickson and Wolf* [1980] suggested that the average quiet tail configuration was inconsistent with simple adiabatic convection. They argued that as plasma convects earthward the plasma pressure will increase until an instability causes the formation of an x line. *Schindler and Birn* [1982] and *Birn and Schindler*, [1983] developed analytic models of quasi-static, time-dependent convection in an asymptotic tail configuration. The only solution they found for steady state, lossless adiabatic convection had the characteristic that field lines in the tail lobes were concave upward. They rejected this configuration as being unphysical and argued, as did *Erickson and Wolf* [1980], that convection will stretch the field lines in the tail leading to tearing-mode reconnection [*Schindler*, 1974]. *Erickson* [1984] and *Hau et al.*, [1989] have built computer models of this process. In particular, *Hau et al.*, [1989] found that while steady convection was indeed possible, it leads to a minimum in the normal component of the magnetic field in the near-earth tail. They argued that within this minimum B region, the tail may become unstable to the tearing mode.

In recent years a number of global magnetohydrodynamic (MHD) simulation models of the solar wind magnetosphere system have been developed [*LeBoeuf et al.*, 1978, 1981; *Lyon et al.*, 1981; *Wu et al.*, 1981; *Brecht et al.*, 1982; *Ogino*, 1986, *Fedder and Lyon*, 1987; *Watanabe and Sato*, 1990]. For southward IMF these models in general have yielded qualitatively consistent results [*LeBoeuf et al.*, 1978; *Lyon et al.*, 1981; *Brecht et al.*, 1982; *Ogino*, 1986; *Watanabe and Sato*, 1990]. They found dayside reconnection followed by nightside reconnection in the plasma sheet. *Lyon et al.*, [1981, 1986] used a two-dimensional model and investigated the effects of resistivity models on the x point in the calculation. They found that the x point stays in the near-earth tail when Joule heating is included in the model but moves tailward in the absence of Joule heating. *Fedder and Lyon* [1987] have identified a driven element in their three-dimensional calculations in which the magnetosphere responds directly to changes in the IMF.

Walker and Ogino [1988] and *Ogino et al.*, [1990*a*] also modeled magnetospheric dynamics following a southward turning of the IMF in three dimensions. They found that when reconnection occurred in the tail, it started near midnight and later spread toward dawn and dusk. The reconnection started on closed field lines and formed a plasmoid tailward of the x line. When reconnection started on lobe field lines, the plasmoid was disconnected from the earth and began to move tailward. *Ogino et al.*, [1990*a*] investigated the effects of the IMF B_y on substorms and found that when $B_y \neq 0$, the plasmoids were configured like twisted flux ropes.

Many of these features also have been studied by using quasi-local MHD models of the magnetotail [*Birn and Hones*, 1981; *Birn*, 1984; *Birn and Hesse*, 1990; *Hesse and Birn*, 1991]. Unlike the global simulations, these codes treat the tail independently of the rest of the magnetosphere. The interfaces to the solar wind and the inner magnetosphere are set by boundary conditions. They, too, found tail reconnection and the formation of plasmoids. When $B_y \neq 0$ they found twisted flux ropes. Recently, *Hesse and Birn* [1991] have noted that the model magnetic field earthward of the reconnection region goes from a taillike to a more dipolar configuration following the onset of reconnection.

In this paper we present the results of a new calculation of the response of the tail to a southward IMF by using a global MHD model. Our emphasis is on the onset of the substorm process. In section 2 we describe the latest version of our global MHD code. The results from the simulation of the temporal evolution of the magnetosphere when the IMF is southward are presented in section 3, while in section 4 we consider the factors which determine when and where reconnection occurs in the simulated tail. Finally, in section 5 we discuss these results in the context of previous theories and observations.

2. The Simulation Model

The latest version of our model has been presented in detail in *Ogino et al.*, [1992] so we will just review its main features here. We have solved the MHD equations and Maxwell's equations as an initial value problem. The normalized resistive MHD equations are the same as those we used in our earlier simulations [*Ogino*, 1986] and are written as follows:

$$\partial\rho/\partial t = -\nabla\cdot(\mathbf{v}\rho) + D\nabla^2\rho$$

$$\partial\mathbf{v}/\partial t = -(\mathbf{v}\cdot\nabla)\mathbf{v} - \nabla P/\rho + (\mathbf{J}\times\mathbf{B})/\rho + \mathbf{g} + \Phi/\rho$$

$$\partial P/\partial t = -(\mathbf{v}\cdot\nabla)P - \gamma P\nabla\cdot\mathbf{v} + D_p\nabla^2 P$$

$$\partial\mathbf{B}/\partial t = \nabla\times(\mathbf{v}\times\mathbf{B}) + \eta\nabla^2 B$$

$$\mathbf{J} = \nabla\times(\mathbf{B} - \mathbf{B}_d)$$

where ρ is the plasma density, $\mathbf{v}$ is the flow velocity, P is the plasma pressure, $\mathbf{B}$ is the magnetic field, $\mathbf{B}_d$ is the intrinsic dipole field of the earth, $\mathbf{J}$ is the current density, $\mathbf{g}$ is the force of gravity, $\Phi = \mu\nabla^2\mathbf{v}$ is the viscosity, $\gamma = 5/3$ is the ratio of specific heats, and η is the resistivity. The resistivity was taken to be uniform throughout the simulation box. We have examined the magnetospheric configuration for $0.0001 \leq \eta \leq 0.002$. The diffusion coefficients are $\mu/\rho_{sw} = D = D_p = 0.001$, where ρ_{sw} is the solar wind density. The magnetic Reynold's number is

$S \equiv \tau_\eta / \tau_A \geq 100$, where $\tau_\eta \equiv \Delta x^2 / \eta$, and $\tau_A = \Delta x / v_A$. Δx is the mesh size and v_A is the Alfvén velocity.

The diffusion and viscous terms were added to suppress MHD fluctuations which come from unbalanced forces at the start of the calculation. These numerical oscillations tend to occur at the bow shock and the magnetopause and have a scale length which is the same as the grid spacing. This does not affect the magnetospheric configuration much because the forces between neighboring meshes tend to cancel each other. The very small viscous and diffusion coefficients used in the calculations are sufficient to suppress these oscillations. This is especially important in the relatively narrow region between the magnetopause and the bow shock where the oscillations can interfere with each other.

In the simulation a uniform solar wind with $n_{sw} = 5/\text{cm}^3$, $v_{sw} = 300$ km/s and $T_{sw} = 2 \times 10^5$°K flows into a simulation box of dimensions $-48R_E \leq x \leq 24R_E$, $0 \leq y \leq 24R_E$, and $0 \leq z \leq 24R_E$ at $x = 24R_E$. Except for temperature, these parameters are on the low side of observed solar wind parameters. The biggest difference is in the solar wind temperature, where our temperature is considerably higher than is typically observed (temperatures as low as 2×10^4°K are frequently found [*Cao*, 1992]). However runs with temperatures as low as 2×10^4°K show that our magnetospheric results are insensitive to temperature [*Chen et al.*, 1992]. Free boundary conditions where the derivatives of all physical quantities are zero, were used at $x = -48R_E$, $y = 24R_E$, and $z = 24R_E$. At $y = 24R_E$ and $z = 24R_E$, the free boundary condition, changes from 90° to the x axis sunward of $x = 0$ to 45° to the x axis at $x = -48R_E$. Mirror boundary conditions were used at $z = 0$ and $y = 0$. The magnetic field of the earth was taken to be a dipole field.

The ionospheric boundary condition imposed near the earth was determined by requiring a static equilibrium [*Ogino*, 1986]. We held all of the model parameters $(\rho, \mathbf{v}, P, \mathbf{B})$ constant for $\xi = (x^2 + y^2 + z^2)^{1/2} < 3.5R_E$. For $3.5R_E < \xi < 5.5R_E$ each parameter ψ was calculated by using

$$\psi = f\psi_{ex} + (1-f)\psi_{in}$$

with

$$f \equiv a_o h / (a_o h + 1)$$

where $a_o = 100$, $h = (\xi / \xi_a)^2 - 1$, and $\xi_a = 3.5R_E$. ψ_{ex} represent the parameter values calculated in the interval $3.5R_E < \xi < 5.5R_E$, while ψ_{in} represents the ionospheric values. In the ionosphere, for $\xi < \xi_a$ we set $h = 0$. This smoothing function damps out all perturbations, including parallel currents, near the ionosphere. Therefore the parallel currents do not close in the ionosphere; rather, they partly close in the smoothing region just above the ionospheric boundary $(\xi = 3.5R_E)$.

The grid was (242,82,82) with a mesh size of $0.3R_E$, and the time step was $\Delta t = 4\Delta x / v_A = 1.12$ s. This ensured that the numerical stability criterion, $v_g^{max} \Delta t / \Delta x < 1$, where v_g^{max} is the maximum group velocity in the calculation domain, was met. In our earlier code [*Ogino*, 1986] the MHD and Maxwell's equations were solved by using the two step Lax-Wendroff method. In the new code we solve the differential equations by

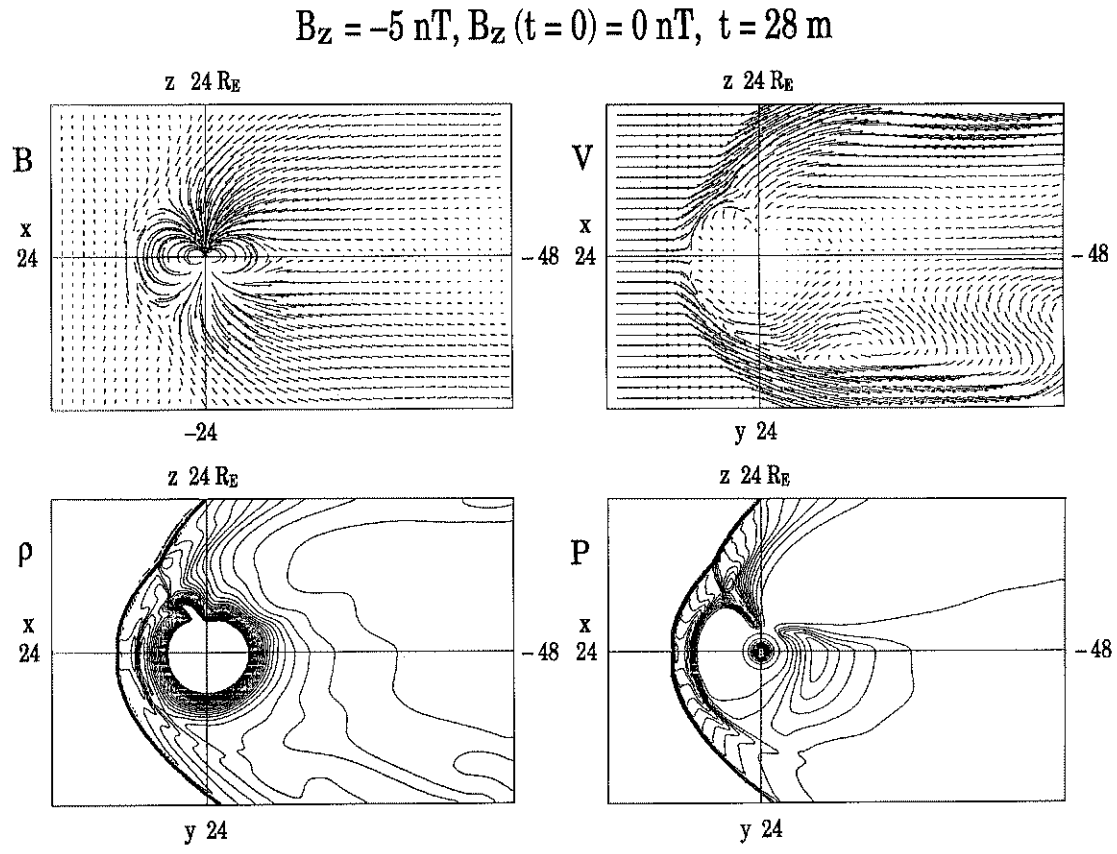

Fig. 1*a*. Magnetic field vectors (**B**), flow velocity vectors (**V**), and density contours (ρ) at t = 28 min after the start of the simulation. The magnetic field vectors are plotted in the noon-midnight meridian. In the inner magnetosphere they are curved along field lines. The length of the arrows gives the field strength at the base of the arrow. Similarly, the flow velocity arrows are curved along flow streamlines. For the flow vectors and the density and pressure contours, the values in the top half of the panel are along the noon-midnight meridian, while those in the bottom half of the figure are in the equatorial plane.

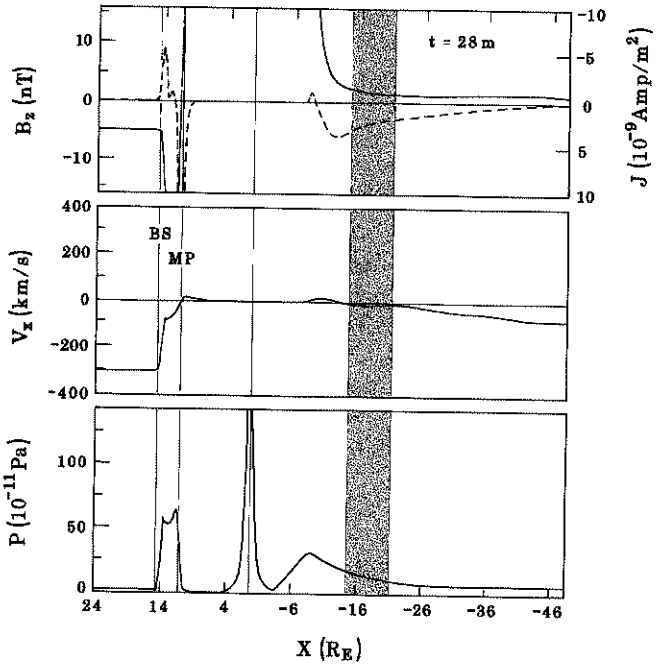

Fig. 1*b*. The component of the magnetic field normal to the equator (B_z), the cross tail current (J_y) (dashed line), the component of the velocity along the earth-sun line (V_x), and the pressure (p) along the earth-sun line (x) at t = 28 min. The shaded area indicates the region in the plasma sheet with southward B_z in Figure 2*b*. On the dayside the bow shock is labeled BS and the magnetopause is labeled MP. Note that the current curve has been inverted, with positive values below the x axis. Positive currents flow duskward.

using a modified version of the leapfrog scheme which is a combination of the leapfrog scheme, and the two step Lax-Wendroff scheme [*Ogino et al.*, 1992].

3. Changes in Magnetospheric Configuration When the IMF Is Southward

At time t = 0, the southward IMF entered the simulation box at its upstream edge. Figures 1–7 show the temporal evolution of the system. In Figure 1*a*, we have plotted magnetic field vectors (**B**), flow vectors (**V**), density contours (ρ), and pressure contours (*P*) 28 min after the southward IMF entered the simulation box. The flow, density, and pressure are plotted such that the top half of each figure corresponds to the noon-midnight meridian, while the bottom half of each figure includes results from the equatorial plane. The magnetic field vectors are confined to the noon-midnight meridian. Values of B_z, the cross tail current (J_y), and *P* along the noon-midnight meridian at this time are plotted in Figure 1*b*. In 28 min the undisturbed solar wind has traveled approximately $84R_E$, which is beyond the end of the simulation box. Reconnection already has started at the subsolar magnetopause but not in the tail. In the plasma sheet (bottom of upper right panel) we see a large viscous cell near the magnetopause but very little convection near midnight. At this time the plasma sheet has a half thickness of about $3R_E$ (Figure 1*a* bottom right panel), and the peak in the tail current is at $x \approx -12R_E$ (Figure 1*b*).

Figure 2 shows the four parameters 10 min later (t = 38 min). There have been several major changes since the last snapshot. In the pressure panel we see that the plasma sheet has started to thin (~$2R_E$ in half-thickness). However, the most dramatic changes have occurred in the equatorial flow pattern (Figure 2*a*). At about $x = -14R_E$, reconnection has started near midnight. Evidence for the tail reconnection is most clearly seen in the equatorial flows, which reverse direction near midnight (Figure 2*a*), and in B_z, which has a southward component for $-14R_E > x > -21R_E$ (Figure 2*b*). Both the earthward and the tailward flows at midnight have velocities of about 50 km/s (Figure 2*b*). Note that reconnection began within about ~$6R_E$ of midnight.

Also evident from Figures 1*a* and 2*a* is the evolution of the plasma mantle-like flow in the lobes of the tail. In Figure 1*a* the flow is mostly tailward, with only a small equatorward component. By the time of Figure 2*a*, the flow has a larger equatorward component and has penetrated about halfway into the lobes.

In Figure 3 we present a three-dimensional view of the magnetic field configuration. The bottom panel contains field lines with at least one end attached to the earth. Here, newly reconnected dayside field lines are characterized by sharp bends. The kink straightens out slowly as the field line is convected tailward. A series of such lines can be seen stretching into the magnetotail and around the dusk magnetopause. This figure demonstrates that convection is a three-dimensional phenomenon even when the IMF is purely southward.

In the top panel of Figure 3, the open field lines in the tail lobes have been removed and magnetosheath field lines have been added. Note that closed field lines extend across the entire width of the plasma sheet. The only indication of the tail reconnection is a small dip in the field lines near midnight that are centered about $x = -14R_E$. The reconnection in Figure 2 started on closed field lines at the equatorial plane. The dip is caused by the convection of closed field lines into the reconnection region.

Figure 4 shows the four parameters at t = 47 min. Now the convection in the lobes extends further into the tail but has not reached the equator in the region modeled by the simulation. The reconnection has continued and has spread across the tail. The earthward flows at midnight have remained at about 50 km/s, while the tailward flows have increased to about 130 km/s (Figure 4*b*). The flows from the reconnection region near the magnetopause have a substantial V_y component as well as tailward or earthward components (Figure 4*a*). Near the boundary they join with the V_y flow from the viscous cells. This results in outward motion of the distant magnetopause. We have found that the magnetic field magnitude is the clearest indicator of magnetopause position in the distant tail. Using the field magnitude, we estimate that between t = 38 min and t = 47 min, the magnetopause at $x = -48\ R_E$ moved from $y = 21\ R_E$ to $y = 23\ R_E$.

At the dayside magnetopause, two small flow vortices have formed. Similar vortices are absent from the flow field at t = 28 min in Figure 1. Careful examination of both the flow field (Figure 2*a*) and the magnetic field indicates that the vortices may just be starting at about 1500 LT or 1600 LT at t = 38 min. (Note that by symmetry, similar waves should be expected on the dawn magnetopause.) We believe that these vortices may be related to the counterstreaming flows at the magnetopause caused by the tail reconnection. Indeed, when we run the simulation with a northward IMF, the strong flows are absent and the vortices at the boundary do not form (see Figure 2*a* of *Ogino et al.* [1992]).

The field lines for this time are plotted in Figure 5. In the top panel, a plasmoid can be seen tailward of the reconnection region. At this time, reconnection is occurring on open lobe field

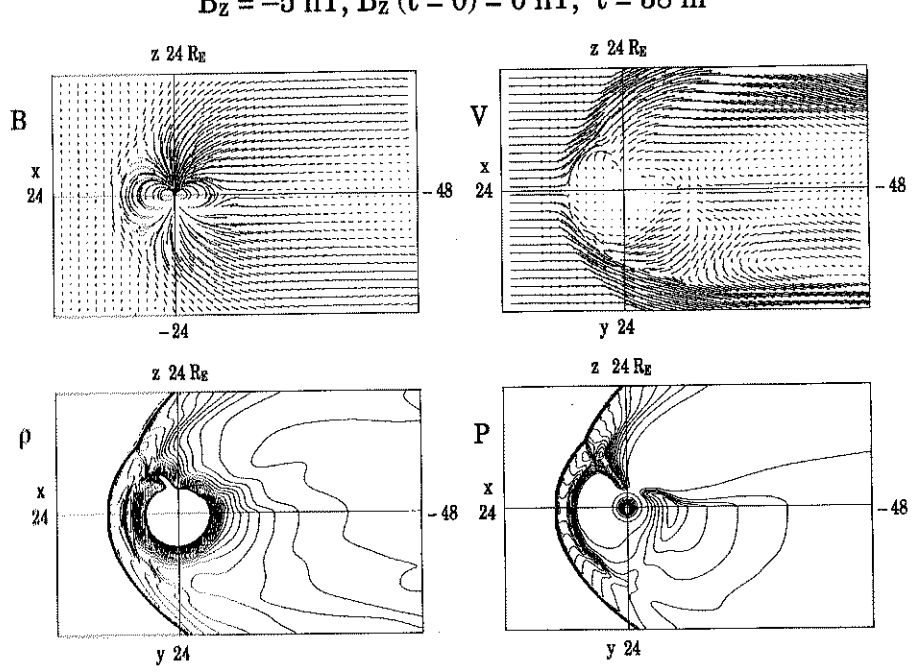

Fig. 2*a*. The same as Figure 1*a* for t = 38 min.

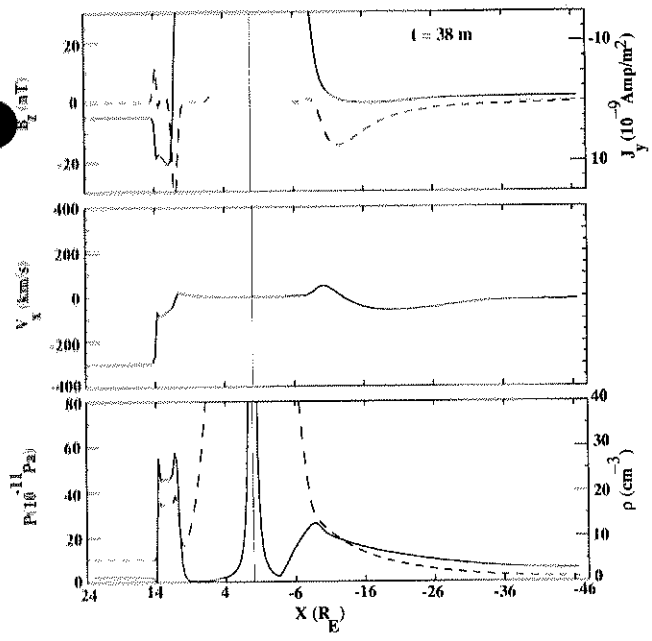

Fig. 2*b*. The same as Figure 1*b* for t = 38 min with the addition of a density curve (dashed line) in the bottom panel.

lines all across the tail. Only a few closed field lines still drape over the plasmoid. Near midnight the plasmoid has started to move tailward. The plasmoid does not begin its motion tailward until the lobe field lines start to reconnect. The plasmoid has a curved footprint in the equatorial plane because it has been moving tailward near midnight for a while but has not started to move nearer to the magnetopause.

The four parameters at the end of the simulation are plotted in Figure 6. In the pressure plot (Figure 6*a*, lower right) the plasmoid can be seen to have moved tailward. The reconnection continues in the near-earth tail, where the tailward flows are now ~150 km/s (Figure 6*b*). The magnetopause has continued to expand in the *y* direction. Unfortunately, it has grown wider than the simulation box and now can be seen exiting the side of the simulation box. The boundary condition at the dusk boundary was not designed for the case where the magnetopause is outside of the simulation box. The boundary condition allows

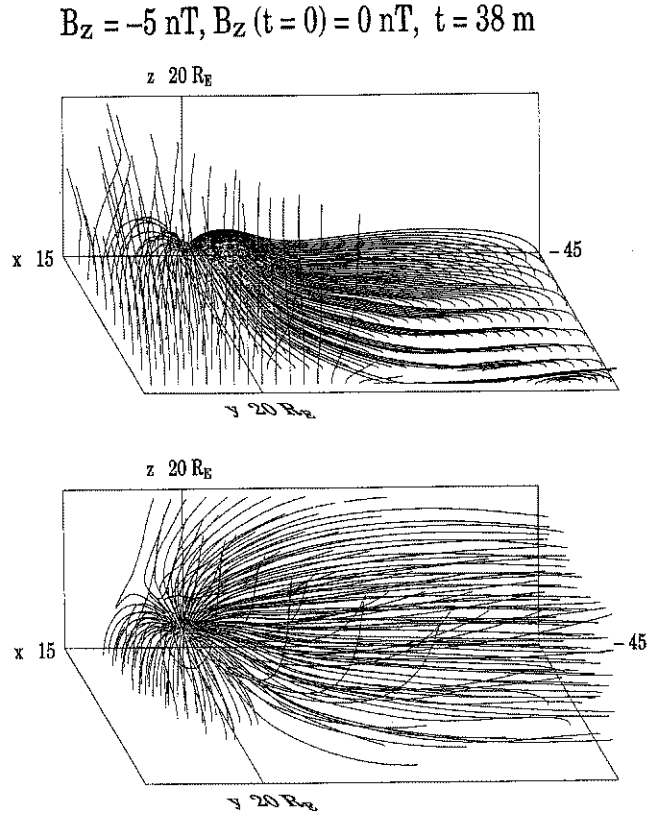

Fig. 3. Magnetic field lines at t = 38 min. In the bottom panel, only field lines attached to the earth are plotted. In the top panel, magnetosheath field lines and closed magnetospheric field lines are plotted.

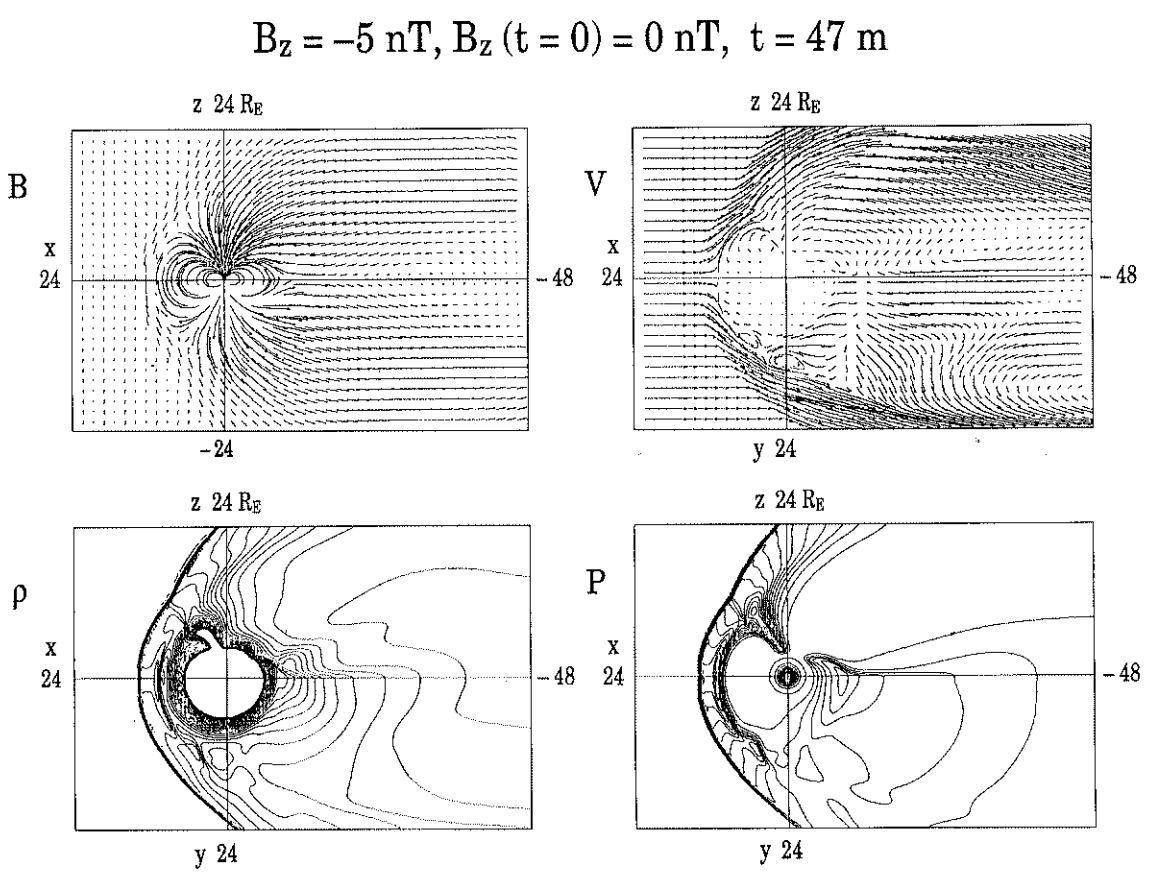

Fig. 4*a*. The same as Figure 1*a* for t = 47 min.

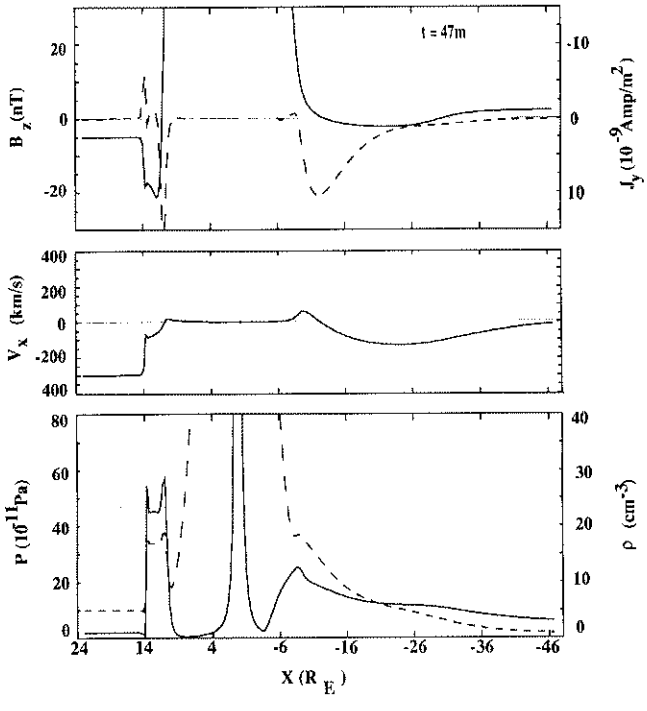

Fig. 4*b*. The same as Figure 2*b* for t = 47 min.

continuous outflow at approximately an angle of 45° to the boundary. While the results should not be trusted in this region, we do not think that this has affected the results in the rest of the magnetosphere, since those results follow continuously from those which occurred before the magnetopause reached the simulation boundary.

In Figure 7 the plasmoid has become completely detached from the Earth and is moving out of the downstream boundary of the simulation box.

In Figure 8 we present another way of visualizing the changes in the magnetospheric configuration during this simulation [*Ogino et al.*, 1990*b*; *N. Nishitani, T. Ogino, and T. Oguti*, unpublished manuscript, 1990]. In the left-hand column we have reproduced the flow pattern in the equatorial plane, while in the right-hand column we have mapped along magnetic field lines from the ionosphere to the magnetosphere. There are two sets of curves in the mapping plots. For one set, called constant-latitude maps, we have calculated the magnetic field lines at all longitudes starting from a fixed latitude on the earth and have drawn a line connecting the equatorial crossing points. These curves are circles near the Earth, since the dipole field dominates there. At higher latitudes the curves are distorted and extend into the tail. For the second set of curves we kept the local time constant and calculated the field lines for different latitudes. These constant-longitude maps are radial in the dipolar field region near the earth but bend and become roughly parallel to the solar wind in the tail. The mapping of any point in the ionosphere to the magnetosphere can be determined from the intersection of the corresponding latitude and longitude curves.

At t = 28 min, prior to the onset of tail reconnection, the 70° field line at midnight connects to a point in the equator at about $x \approx -25\ R_E$, while the 71° field line connects to nearly the end of the simulation box ($x \approx -45\ R_E$). Between 28 min and 38 min the plasma sheet has thinned so that the 70° field line extends to the end of the box at $x = -48\ R_E$. Nearer the Earth there is a "hole" in the map. No closed field lines connect to this region, which is occupied by the plasmoid. That the reconnection starts in a small region near midnight is most clearly seen in this display. By t = 47 min the reconnection has moved across the

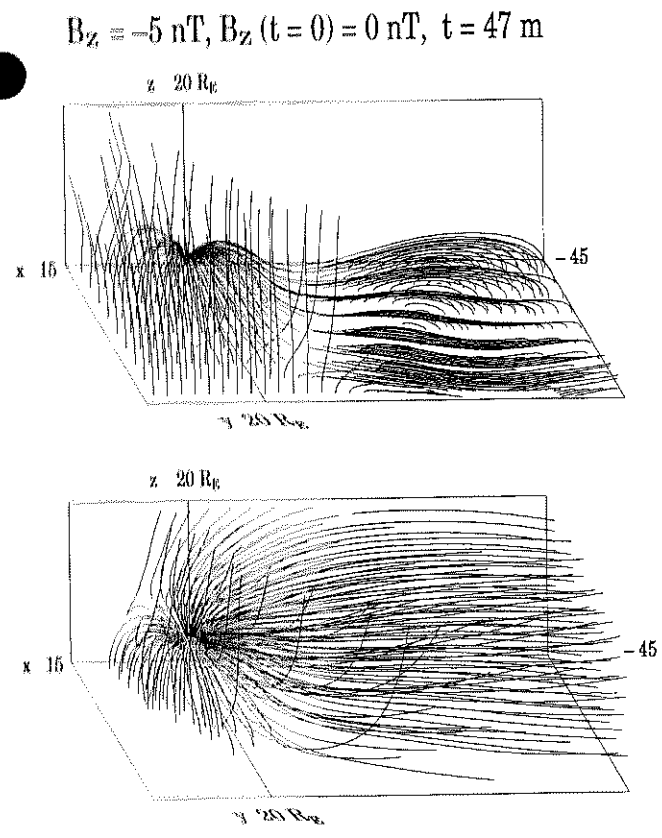

Fig. 5. The same as Figure 3 for t = 47 min.

tail and only a few closed field lines still map to the downstream boundary. Finally, by t = 57 min all of the closed field lines have been reconnected and the "hole" includes the entire magnetotail tailward of the x line.

4. Formation of the Near-Earth Neutral Line

In this section we will discuss the factors which control reconnection in the simulation and the reasons that the tail reconnection occurs in the near-earth region. To help us better understand the parameters which control the reconnection in our simulation, we examined the results from a second run. The only difference between this run and the first was the length of the tail. In this case the tail was 25 R_E in length rather than 48 R_E. In Figure 9 we have plotted the four parameters at t = 40 min during the shorter-tail simulation. Tail reconnection has not yet begun in this simulation. The plasma sheet is still thick (the half-thickness $\Delta z \sim 5R_E$) with a large B_z. In the longer-tail case, reconnection had already begun at this time. The important features of this run are summarized in Figure 10, where the V_x and B_z components at midnight at $x = -16\ R_E$ have been plotted versus time. As in the first case, reconnection in this run occurred in the near-earth tail between $x = -12\ R_E$ and $x = -14 R_E$. However, it took at least 30 min longer (between 64 min and 84 min) for reconnection to start in the second case than in the first case. We believe that this delay is due to the difference in the component of the magnetic field (B_z) normal to the equator. Studies of tearing-mode reconnection have shown that the normal component of **B** can stabilize the mode [*Schindler*, 1974; *Galeev and Zelenyi*, 1976; *Lembege and Pellat*, 1982]. In Figure 10 at t = 40 min, $B_z \sim 5nT$. At the same location in the longer tail simulation, $B_z \sim 2nT$ at t = 28 min (see Figure 1*b* top panel). The time difference seems to be related to the time it takes to reduce B_z sufficiently for the tail to become unstable to the tearing mode. The observation that the reconnection first occurs near midnight also supports this idea, since B_z is smaller in the central part of the tail than near the magnetopause.

In addition to the two runs we discussed above, we also have run the code with a solar wind velocity of 600 km/s and an IMF of $B_z = -10$ nT. For this run too the tail reconnection occurred at $x \approx -14\ R_E$.

Why does the reconnection occur in the near tail rather than deeper in the tail? In Figure 11, contour plots of the total pressure (magnetic plus thermal) at each time step are in the left-hand column, while vector plots of the Poynting fluxes ($\mathbf{E}\times\mathbf{B}/\mu_o$) at the same times are in the right-hand column. For both of these parameters the top of each plot shows the values in the noon-midnight meridian, while the equatorial plane values are at the bottom. As noted above, the reconnection occurs at $x = -14\ R_E$. This is at the intersection of the region dominated by the dipole field and the region dominated by the tail and is characterized by a large north-south gradient in the total pressure.

On the dayside, the energy flux onto the magnetosphere is deflected along the magnetopause by reconnection. This deflection appears as a line of arrows along the magnetopause in the Poynting flux plots. In the tail the Poynting flux reaches the equator first in the critical near-earth region (t = 28 min), where it causes the required plasma sheet thinning and reconnection (t = 38 min). Later, after tail reconnection has begun, the Poynting flux near the equator is in both directions away from the x line (t = 47 min and t = 57 min).

The divergence of the Poynting flux ($\boldsymbol{S}$) can be expressed as

$$\nabla\cdot\boldsymbol{S} = \frac{-1}{2\mu_o}\frac{\partial B^2}{\partial t} - \mathbf{J}\cdot\mathbf{E}.$$

The first term on the right is the rate of change of magnetic energy, while the second term gives the rate of change of magnetic to plasma energy. In Figure 12 we have plotted the change in B^2 between t = 28 min and t = 47 min in the top panel and the change between t = 47 min and t = 57 min in the bottom panel. In the interval between t = 28 min and t = 47 min, the magnetic flux into the tail lobes increased ($\Delta B^2 \sim 200nT^2$). This is the interval of plasma sheet thinning and reconnection on closed field lines. In contrast, during the interval from t = 47 min to t = 57 min, when lobe field lines were reconnecting, the lobe field remained nearly constant ($\Delta B^2 \sim 10nT^2$ throughout much of the tail lobes). The reconnection was returning flux to the dayside about as fast as it was being transported into the tail.

Figure 13 shows **J** and **E** and $\mathbf{E}\times\mathbf{B}/\mu_o$ along the noon-midnight meridian for five times. $\mathbf{J}\cdot\mathbf{E}$ is negative at the bow shock, where solar wind energy is transformed into magnetic energy, and positive at the magnetopause, where magnetic energy is going into the plasma. Note that the magnetopause moves earthward during the simulation. This movement is caused by the erosion of the magnetopause position by the reconnection. The most dramatic time changes occur in the near-earth tail. Here, $\mathbf{J}\cdot\mathbf{E}$ is again positive as magnetic energy is changed into plasma energy. It decreases in the tail between t = 19 min and t = 28 min prior to the onset of reconnection and then increases between t = 38 min and t = 57 min after tail reconnection starts. $\mathbf{J}\cdot\mathbf{E}$ is largest at t = 57 min after the tail lobe field lines have begun to reconnect.

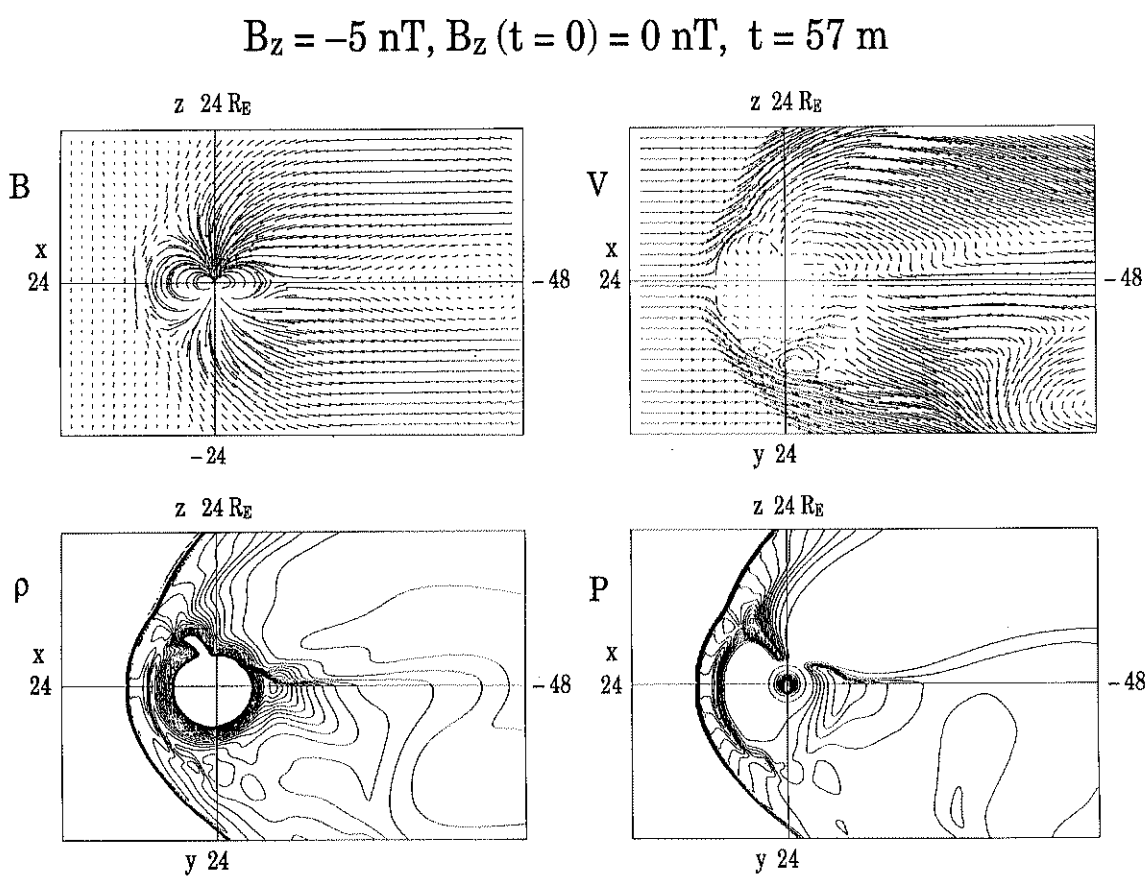

Fig. 6*a*. The same as Figure 1*a* for t = 57 min.

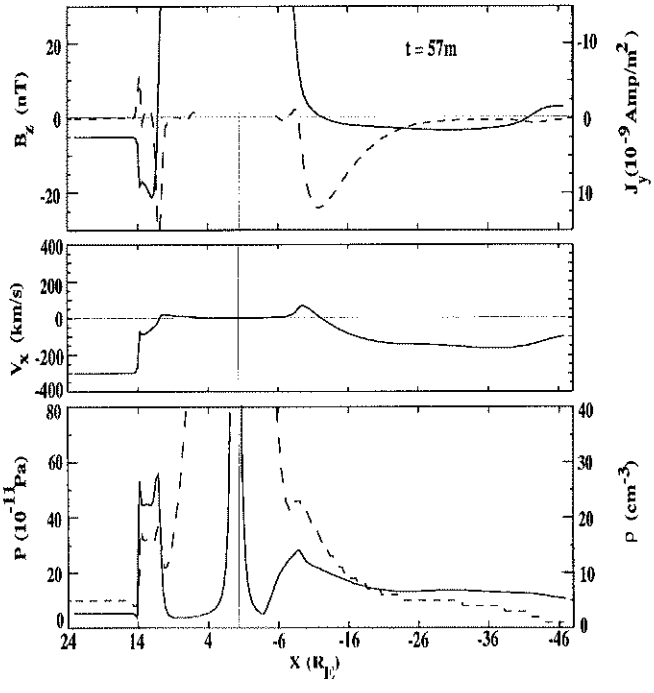

Fig. 6*b*. The same as Figure 2*b* for t = 57 min.

5. Discussion and Summary

In general our simulation results for southward IMF are consistent with the expectations of the near-earth neutral-line model of substorms. After the southward IMF reaches the dayside magnetopause, reconnection begins and magnetic flux is convected into the tail lobes. After about 35 min, reconnection begins within the plasma sheet near midnight at $x = -14\ R_E$. Later, the x line moves towards the dawn and dusk magnetopause. When the plasma sheet field lines have reconnected, the reconnection begins on lobe field lines, freeing the plasmoid to move down the tail under the influence of the tension on reconnected lobe field lines. These results are similar to those we found with an earlier much lower resolution ($\Delta x = 1\ R_E$) model [*Walker and Ogino*, 1988].

Earthward of the reconnection region, the equatorial magnetic field becomes more dipolar following the onset of reconnection. For this case at $x = -9R_E$, $B_z \approx 9nT$ at t = 47min (Figure 4*b*) and $B_z \approx 11nT$ at t = 57 min (Figure 6*b*). These results are similar to those of Hesse and Birn (1991) but are less dramatic. As in the *Hesse and Birn* [1991] simulation, this dipolarization effect is primarily caused by the effects of the ionospheric boundary condition, which effectively starts at $r = 5.5R_E$. This conducting obstacle limits the inward motion of the plasma and allows the field to pile up.

In the simulation the plasma sheet thinning is associated with an increase in the cross-tail current, while in the near-earth neutral-line model the current region is thought to move earthward as well as increase. Again, since the earthward motion of the fluid in the simulation is limited by the line tieing of the ionospheric boundary condition, the inward motion of the current system is restricted as well. The large radial extent of the ionospheric boundary also causes us to find larger-than-observed densities in the near-tail region. For instance, at $x = -15R_E$ the density is about 5 cm^{-3}, while typical observed values are 1 cm^{-3}

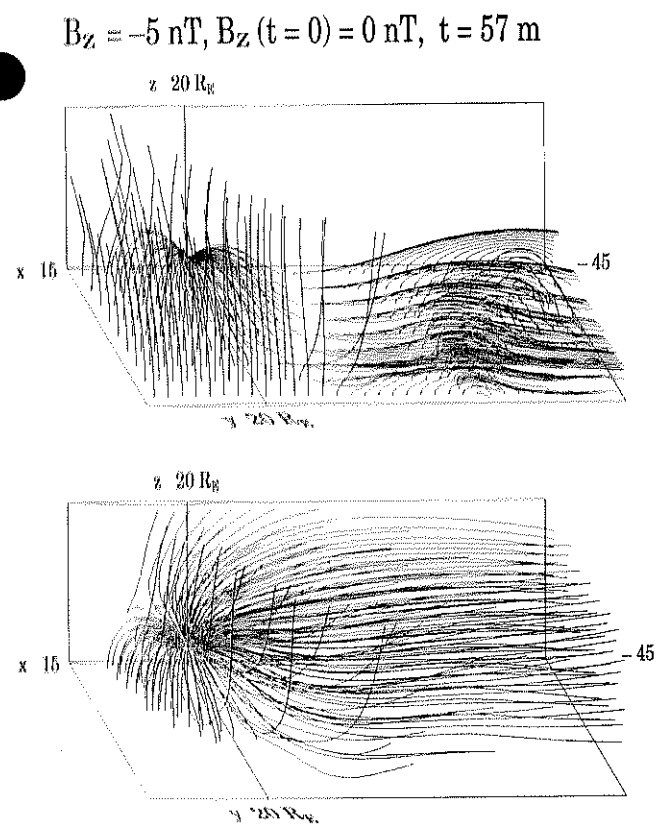

Fig. 7. The same as Figure 3 for t = 57 min

or less [see *Frank*, 1985, for a review]. This may have caused the earthward flow to divert around the obstacle tailward of where it would have with a more realistic inner magnetosphere and may affect the location of reconnection. This reduction in earthward v_x also explains why the dipolarization is less dramatic in our simulation than in that of *Hesse and Birn* [1991].

In the near-earth neutral-line model of substorms the onset of the expansion phase is attributed to reconnection on open field lines. Reconnection, however, must begin on closed plasma sheet field lines, and this necessity has caused a problem for the near-earth neutral-line model. There is no observational evidence for tail reconnection during the substorm growth phase. Proponents of the near-earth neutral-line model have argued that the interval of plasma sheet reconnection is very short (a few minutes, *Hones et al.* [1986]), that it is too slow to cause observable effects until open field lines become involved or that the reconnection region is very localized [*McPherron*, 1990]. In the simulation the reconnection on closed field lines can last a long time. It lasted ~15 min in this case, and we have found cases where it lasted 30 min or more depending on the initial configuration in the plasma sheet. That the simulated plasma sheet reconnection starts in a localized region gives some support to the last suggestion. However, in the simulation the reconnection on closed field lines has many of the features associated with the substorm expansion, including relatively strong flows and dipolarization of the field earthward of the reconnection site. Thus the results suggest that the expansion phase begins earlier in the sequence of events then in the most common version of the near-earth neutral-line model. The period of plasma sheet reconnection is sufficiently long that we can imagine events in which the substorm sequence ends before lobe field lines start reconnecting. It would be interesting to test this idea by running a simulation in which the IMF is turned northward before tail lobe reconnection begins. This possibility is beyond the scope of this paper.

For all of our runs the neutral line formed at approximately the same location in the near-earth plasma sheet. That location is determined by the energy flux into the tail following the dayside reconnection. During the growth phase the Poynting flux is concentrated in the region where the tail attaches onto the magnetic-dipole-dominated inner magnetosphere. For constant solar wind input parameters, the delay between the start of simulation and the onset of reconnection was determined by the size of the normal component B_z of the magnetic field across the equator. Reconnection began after B_z was reduced sufficiently for the tearing mode to grow.

The results presented here on the location of reconnection seem to be consistent with the conclusions of some observational studies such as those of the first CDAW-6 substorm [*McPherron*, 1990]. However, other studies indicate that this is not always the case and that reconnection usually occurs tailward of $20R_E$ [*Cattell and Mozer*, 1984; *Huang and Frank*, 1986; *Baumjohann et al.*, 1989]. The location of reconnection remains an area of controversy and intense observational study.

The simulation results do not appear to be consistent with the model that plasma sheet convection is the cause of the near-earth neutral line [*Erickson and Wolf*, 1980; *Erickson*, 1984; *Hau et al.*, 1989]. In the simulation, most of the flow prior to the onset of reconnection is on the flanks of the magnetosphere near the magnetopause (Figure 1*a*) and the earthward convection near midnight is small (<15 km/s in Figure 1*b*). This convection does not appear to be large enough to cause the local minimum in B_z required by the convection theory.

Near the end of this simulation the flow from the tail reconnection exited the sides of the simulation box. Subsequent to submitting this paper for publication, we ran the simulation with a wider ($40R_E$) and longer ($160R_E$) simulation box. The sequence of events in this simulation were the same as those reported here. In this calculation a solar wind without an IMF entered the simulation box at t = 0. Two hours later, a southward IMF entered the box. In Figure 14 we have plotted the four parameters 60 min after the southward IMF entered the box. As before, the reconnection started in the near-earth tail. The flow from the reconnection region is tailward and toward dawn, just as in the case with the $48R_E$ tail. This time, however, the flow is contained within the box and the magnetosphere (cf. Figure 6*a* and Figure 14). Note that in the longer-tail run, the tailward velocities are slightly higher (~200 km/s) than in the previous runs.

In both our simulation and those of *Birn* [*Birn*, 1984; *Birn and Hones*, 1981], the tail reconnection leads to a tailward moving plasmoid. In the Birn model it is flow from the reconnection that causes the plasmoid to move tailward. In our calculation an added contribution from the tension on reconnected field lines seems to be necessary for the plasmoid to move tailward, since the plasmoid does not start its tailward motion until lobe field lines are reconnected.

So far we have started the simulation runs either by allowing a southward IMF to interact with a dipole magnetic field to form a rapidly evolving magnetosphere or by allowing a southward IMF to interact with the magnetosphere formed without an IMF. In the real magnetosphere the southward IMF interacts with a magnetosphere which has already formed in the presence of an

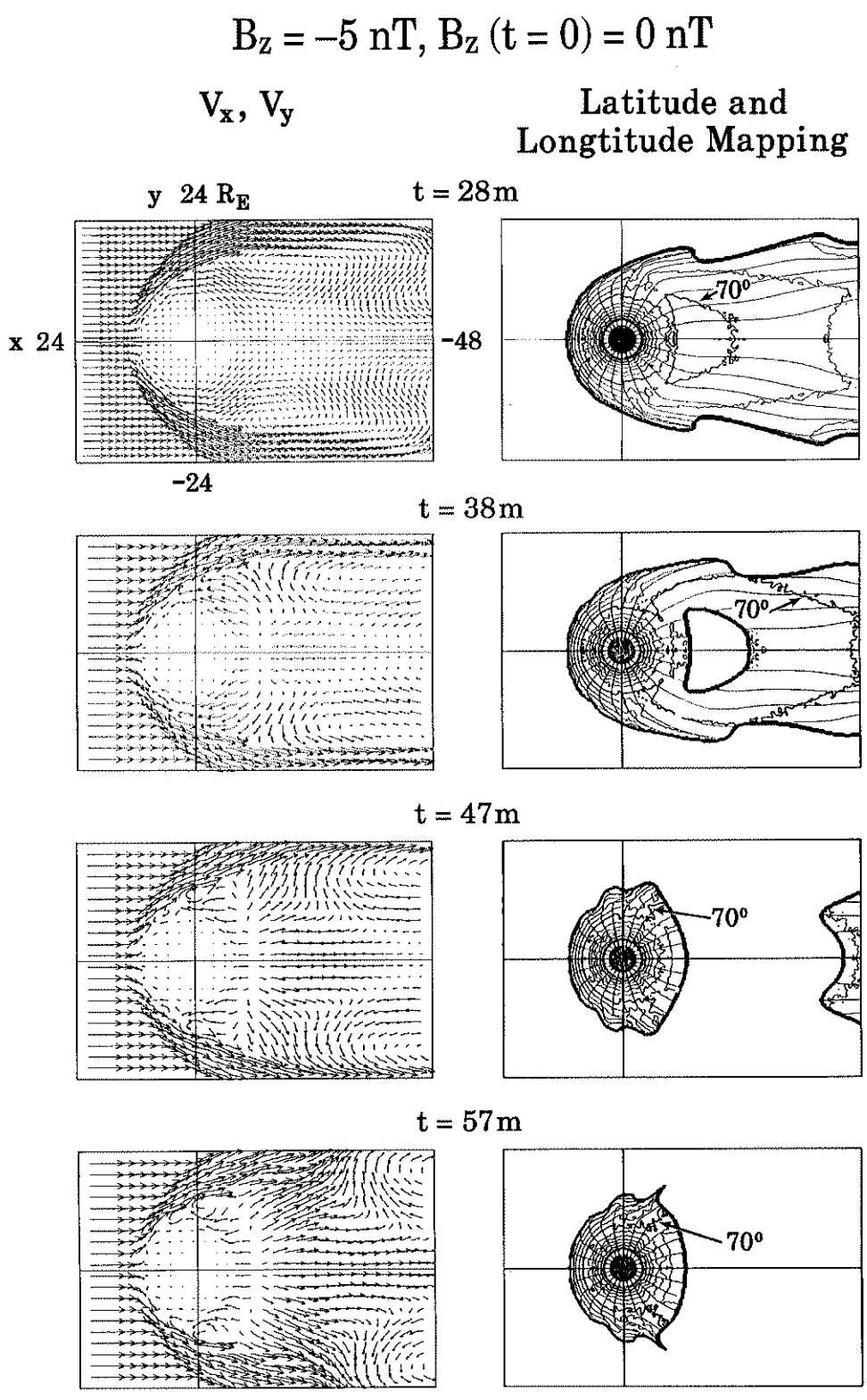

Fig. 8. Flow vectors (V_x,V_y) in the equatorial plan (left) and field line mappings (right) for t = 28 min, 38 min, 47 min, and 57 min. There are two types of mapping curves. For one type, field lines were traced from the ionosphere to the equator at constant latitude and all longitudes. The resulting curves are circles near the earth and are stretched out into the tail on the nightside. The second set of curves was calculated by keeping the local time constant and changing the latitude. Near the earth these curves are radial, but in the outer magnetosphere they bend approximately parallel to the solar wind. No field lines map from the earth to the equator in the blank areas such as the region near midnight in the near-earth tail at t = 38 min. The field lines in this region have reconnected.

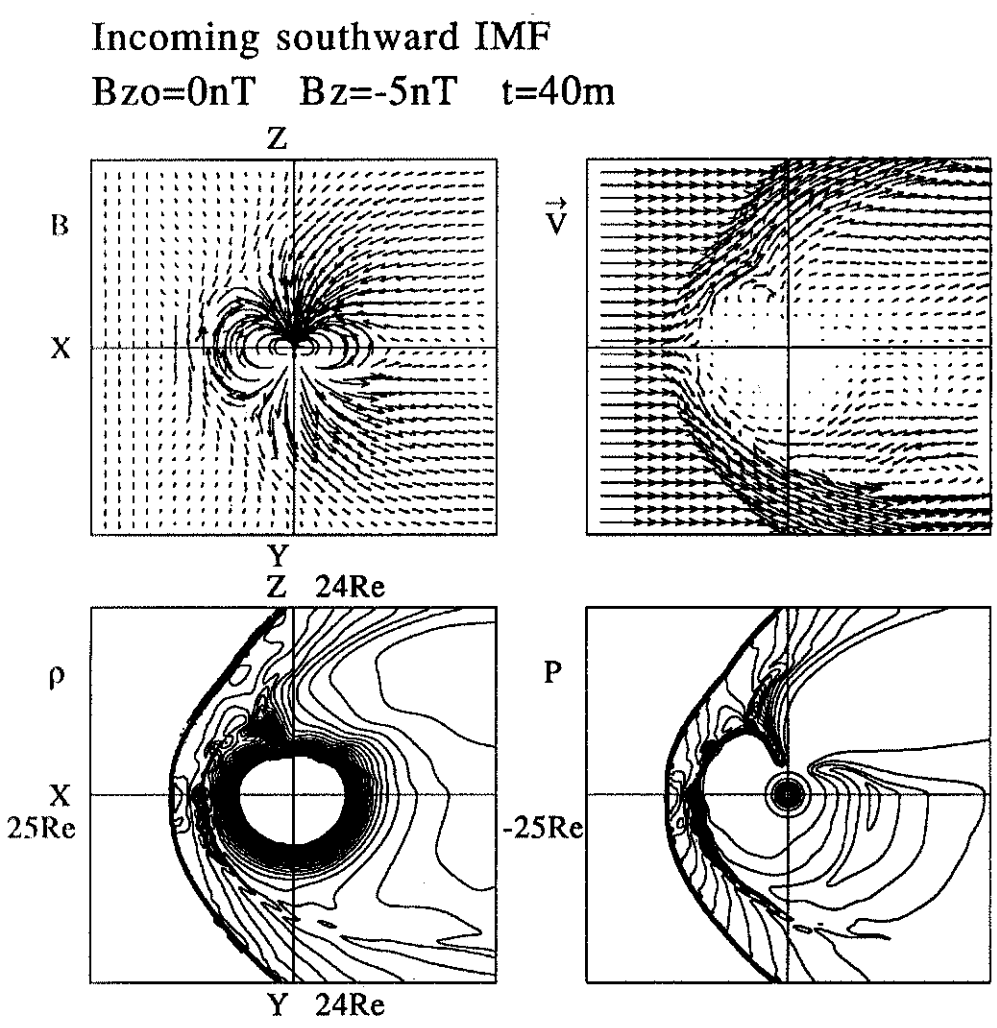

Fig. 9. The same as Figure 1*a* for the short-tail (25 R_E) simulation at t = 40 min.

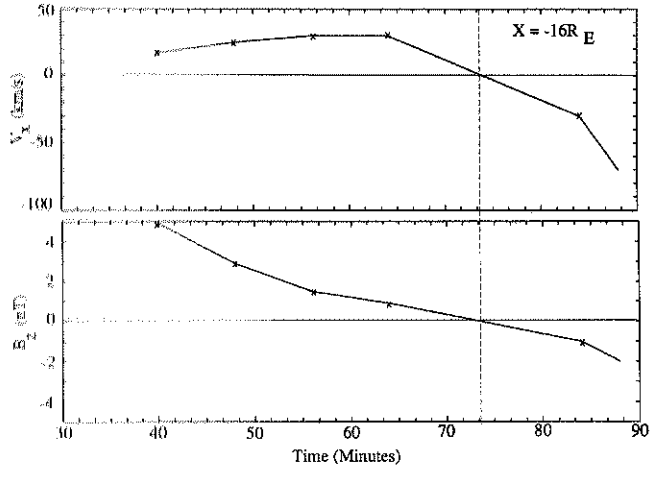

Fig. 10. The component of the flow velocity along the earth-sun line (V_X) and the component of the magnetic field normal to the equator (B_Z) versus time at $x = -16R_E$, $y = 0$, $z = 0$ from the short tail version of the code. The dashed line at t = 74 min is an estimate of the time at which reconnection began. The x marks show the times for which results are available.

IMF. In some cases this is a magnetosphere formed while the IMF was northward, while in others it is the magnetospheric configuration of an ongoing substorm. Our next step in this study will be to carry out a simulation parameter search in which we vary the initial conditions of the simulation. This may help us understand some of the outstanding questions asked above. It may help us understand the apparently contradictory observations concerning the location of the onset of reconnection. It may help us determine if there are conditions with strong flows in the center of the plasma sheet such that the plasma sheet convection model of substorms is applicable. Finally, it may help us determine if there are periods of enhanced convection for southward IMF without substorms and reconnection [*Pytte et al.*, 1978; *Sergeev and Lennartsson*, 1988].

Another aspect of substorm phenomena not included in our simulation is the recovery phase. In the near-earth neutral-line model, the recovery phase is associated with the tailward retreat of the near-earth neutral line. As the neutral line moves tailward, the plasma sheet refills behind it. This, too, awaits further simulation studies.

$B_z = -5$ nT, B_z (t = 0) = 0 nT

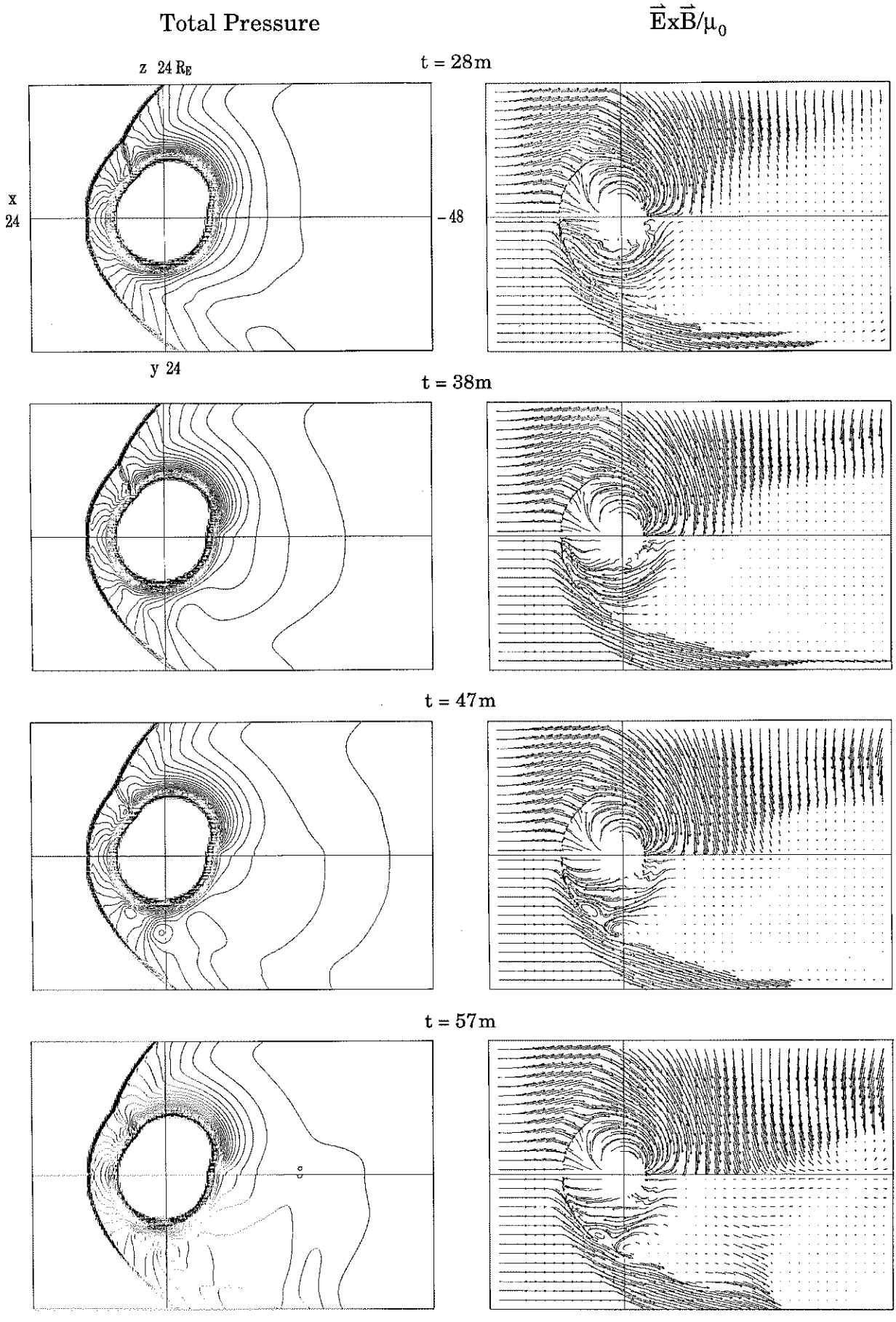

Fig. 11. Contours of total pressure ($B^2/2\mu_0 + nkT$) and the Poynting flux ($\mathbf{E} \times \mathbf{B}/\mu_0$) for t = 28 min, 38 min, 47 min and 57 min. The top of each panel gives the values in the noon-midnight meridian while the bottom shows the values in the equatorial plane.

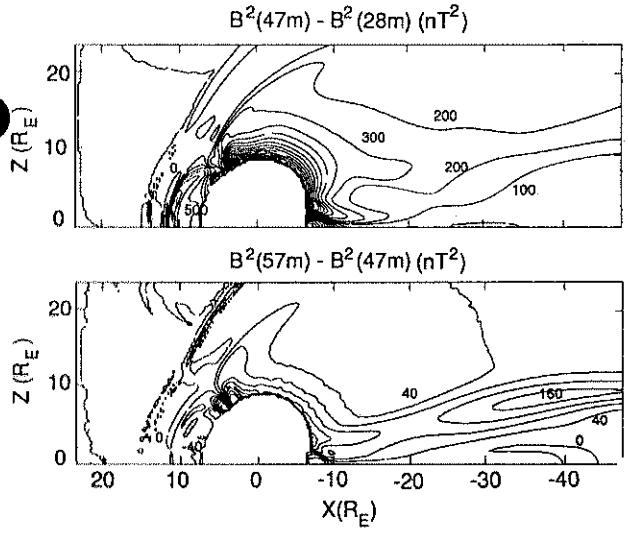

Acknowledgments. We gratefully acknowledge helpful discussions with M. G. Kivelson, F. V. Coroniti, and R. L. Richard. The work at UCLA was supported by NASA Space Physics Theory Program grant NAG5-1480 and NASA International Solar Terrestrial Physics Program grant NAG5-1100. The work at Nagoya University was supported by a grant in aid for science research from the Ministry of Education, Science and Culture. Computing support for our simulations was provided by the San Diego Supercomputer Center and by the Computer Center of Nagoya University. Institute of Geophysics and Planetary Physics publication number 3666.

The Editor thanks R. E. Lopez and J. G. Lyon for their assistance in evaluating this paper.

Fig. 12. The change in B^2 between t = 28 min and t = 47 min (top) and t = 47 min and t = 57 min (bottom). The contour intervals are $100nT^2$ at the top and $40nT^2$ at the bottom. Areas with $B > 100nT$ were excluded from the plot.

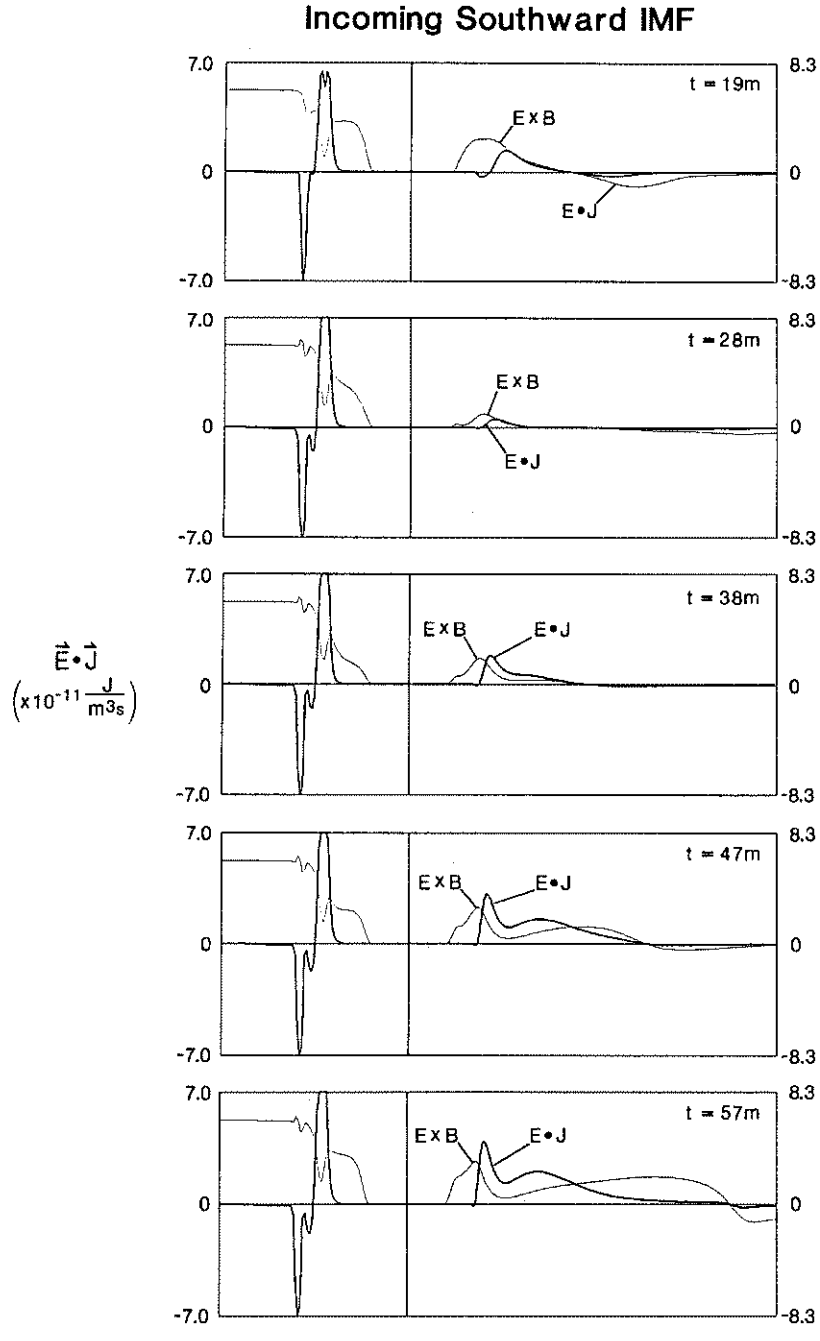

Fig. 13. $\mathbf{J} \cdot \mathbf{E}$ (heavy line) and $\mathbf{E} \times \mathbf{B}/\mu_0$ (light line) along the sun-earth line for five times (t = 19 min, 28 min, 38 min, 47 min, and 57 min).

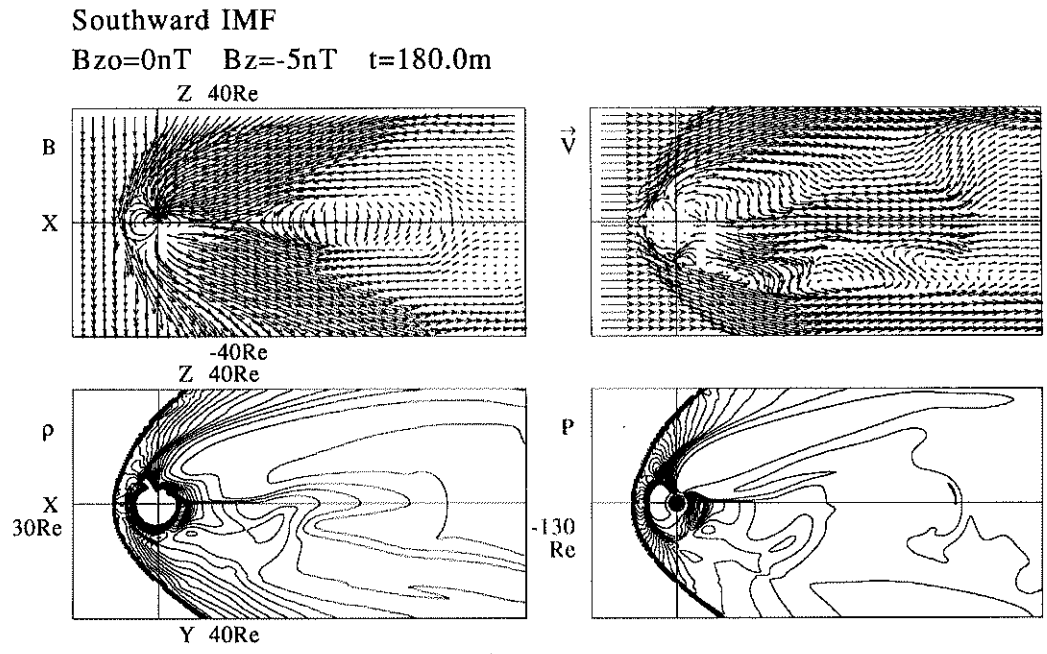

Fig. 14. The same as Figure 1*a* for the long-tail ($130R_E$) model at 60 min after the southward interplanetary magnetic field entered the simulation box.

REFERENCES

Akasofu, S. -I., Energy coupling between the solar wind and the magnetosphere, *Space Sci. Rev.*, *28*(121), 1981*a*.

Akasofu, S. - I., Magnetospheric substorms: A newly emerging model, *Planet. Space Sci.*, *29*(10), 1069, 1981*b*.

Akasofu, S. -I., D.S. Kimbal and C.-I. Meng, Dynamics of the aurora, 2, westward traveling surges, *J. Atmos. Terr. Phys.*, *27*, 173, 1965.

Akasofu, S. -I., D. S. Kimbal and C. -I. Meng, Dynamics of the aurora, 4, *J. Atmos. Terr. Phys.*, *28*, 489, 1966.

Baker, D. N., Particle and field signatures of substorms in the near magnetotail, in *Magnetic Reconnection in Space and Laboratory Plasmas*, *Geophys. Monogr. Ser.*, vol. 30, edited by E. W. Hones, p. 193, AGU, Washington, D.C., 1984.

Baumjohann, W., G. Paschmann, and C. A. Cattell, Average plasma properties in the central plasma sheet, *J. Geophys. Res.*, *94*, 6597, 1989.

Birn, J., Three-dimensional computer modeling of dynamic reconnection in the magnetotail: Plasmoid signatures in the near and distant tail, in *Magnetic Reconnection in Space and Laboratory Plasmas, Geophys. Monogr. Ser.*, vol. 30, edited by E. W. Hones, p. 264, AGU, Washington, D.C., 1984.

Birn, J., and M. Hesse, The magnetic topology of the plasmoid flux rope in a MHD simulation of magnetotail reconnection, in *Physics of Magnetic Flux Ropes*, *Geophys. Monogr. Ser.*, vol. 58, edited by C. T. Russell, E. R. Priest, and L. C. Lee, p. 655, AGU, Washington, D. C., 1990.

Birn, J., and E. W. Hones, Jr., Three dimensional computer modeling of dynamic reconnection in the geomagnetic tail, *J. Geophys. Res.*, *86*, 6802, 1981.

Birn, J., and K. Schindler, Self-consistent theory of three-dimensional convection in the geomagnetic tail, *J. Geophys. Res.*, *88*, 6969, 1983.

Brecht, S. H., J. G. Lyon, J. A. Fedder and K. Hain, A time dependent three dimensional simulation of the earth's magnetosphere: Reconnection events, *J. Geophys. Res.*, *87*, 6098, 1982.

Cao, M., ULF waves in the earth's dayside magnetosphere, PHD thesis, Univ. of Calif., Los Angeles, 1992.

Cattell, C. A., and F. S. Mozer, Substorm electric fields in the Earth's magnetotail, in *Magnetic Reconnection in Space and Laboratory Plasmas*, *Geophys. Monogr. Ser.*, vol. 30, edited by E. W. Hones, p. 208, AGU, Washington, D. C., 1984.

Chen, S. -H., M. G. Kivelson, J. T. Gosling, R. J. Walker, and A. J. Lazarus, Anomalous aspects of magnetosheath flow and the shape and oscillations of the magnetopause during an interval of strongly northward interplanetary magnetic field, *J. Geophys. Res.*, *98*, 5727, 1993.

Craven, J. D., and L. H. Frank, Latitudinal motion of the aurora during substorms, *J. Geophys. Res.*, *92*, 4565, 1987.

DeForest, S., and C. E. McIlwain, Plasma clouds in the magnetosphere, *J. Geophys. Res.*, *76*, 3587, 1971.

Elphinstone, R. D., D. Hearn, J. S. Murphree,and L. L. Cogger, Mapping using the Tsyganenko long magnetospheric model and its relationship to Viking auroral images, *J. Geophys. Res.*, *96*, 1467, 1991.

Erickson, G. M., On the cause of x-line formation in the near-earth plasma sheet: Results of adiabatic convection of plasma sheet plasma, in *Magnetic Reconnection in Space and Laboratory Plasmas*, *Geophys. Monogr. Ser.*, vol. 30, edited by E. W. Hones, p. 296, AGU, Washington, D.C., 1984.

Erickson, G. M., and R. A. Wolf, Is steady convection possible in the earth's geomagnetic tail?, *Geophys. Res. Lett.*, *7*, 897, 1980.

Fedder, J. A., and J. G. Lyon, The solar wind-magnetosphere-ionosphere current voltage relationship, *Geophys. Res. Lett.*, *14*, 880, 1987.

Frank, L. H. Plasmas in the Earth's magnetotail, in *Space Plasma Simulations*, edited by M. Ashour-Abdalla and D. A. Dutton, p. 211, D. Reidel, Norwell, Mass., 1985.

Galeev, A. A., and L. M. Zelenyi, Tearing instability in plasma configuration, *Sov. Phys. JETP*, Engl. Trans., *43*, 1113, 1976.

Goertz, C. K., and R. A. Smith, Thermal catastrophe model of substorms, J. Geophys. Res., 94, 593, 1989.

Hau, L.-N., R. A. Wolf, G.-H. Voigt, and C. C. Wu, Steady state magnetic field configurations for the earth's magnetotail, *J. Geophys. Res.*, *94*, 1303, 1989.

Hesse, M., and J. Birn, On dipolarization and its relation to the substorm current wedge, *J. Geophys. Res.*, *96*, 19,427, 1991.

Hones, E. W., Jr., J. R., Asbridge, S. J. Bame, and S. Singer, Substorm variations of the magnetotail plasma sheet from $x_{sm} = -6R_E$ to $x_{sm} = -60R_E$, *J. Geophys. Res.*, *78*, 109, 1973.

Hones, E. W., Jr., D. N. Baker, W. C. Feldman, J. T. Gosling, D. J. McComas, R. D. Zwickl, J. A. Slavin, E. J. Smith, and B. T. Tsurutani, Structure of the magnetotail at 220 R_E and its response to geomagnetic activity, *Geophys. Res. Lett.*, *11*, 5, 1984.

Hones, E. W., Jr., T. Fritz, J. Birn, J. Cooney, and S. J. Bame, Detailed observations of the plasmasheet during a substorm on April 24, 1979, *J. Geophys. Res.*, *91*, 6845, 1986.

Huang, C. Y., and L. A. Frank, A statistical study of the central plasma sheet: Implications for substorm models, *Geophys. Res. Lett.*, *13*, 7, 652, 1986.

Kaufmann, R., L., Substorm currents: growth phase and onset, *J. Geophys. Res.*, *92*, 7471, 1987.

Kokubun, S., and R. L. McPherron, Substorm signatures at synchronous altitude, *J. Geophys. Res.*, *86*, 11,265, 1981.

LeBoeuf, J. N., T. Tajima, C. F. Kennel, and J. M. Dawson, Global

simulation of the time-dependent magnetosphere, *Geophys. Res. Lett., 5*, 609, 1978.

LeBoeuf, J. N., T. Tajima, C. F. Kennel, and J. M. Dawson, Global simulation of the three-dimensional magnetosphere, *Geophys. Res., Lett., 8*, 257, 1981.

Lembege, B., and R. Pellat, Stability of a thick two-dimensional quasi-neutral sheet, *Phys. Fluids, 25*, 1995, 1982.

Lopez, R. E., D. N. Baker, A. Y. T. Lui, D. G. Sibeck, R. D. Belian, R. W. McEntire, T. A. Potemra, and S. M. Krimigis, The radial and longitudinal propagation characteristics of substorm injections, *Adv. Space Res., 8*(9), 91, 1988*a*.

Lopez, R. E., A. T. Y. Lui, D. G. Sibeck, R. W. McEntire, L. J. Zanetti, T. A. Potemra, and S. M. Krimigis, The longitudinal and radial distribution of magnetic reconfigurations in the near-earth magnetotail as observed by AMPTE/CCE, *J. Geophys. Res., 93*, 997, 1988*b*.

Lui, A. T. Y., C.-L. Chang, A. Mankofsky, H.-K. Wong, and D. Winske, A cross-tail current instability for substorm expansions, *J. Geophys. Res., 96*, 11389, 1991.

Lyon, J. G., S. H. Brecht, J. D. Huba, J. A. Fedder, and P. J. Palmadesso, Computer simulation of a geomagnetic substorm, *Phys. Rev. Lett., 46*, 1038, 1981.

Lyon, J. G., J. A. Fedder, and J. D. Huba, The effects of different resistivity models on magnetotail dynamics, J. Geophys. Res., 91, A7, 8057, 1986.

McPherron, R. L., Physical processes producing magnetospheric substorms and magnetic storms, *Geomagnetism, 4*, 593, 1990.

McPherron, R. L., C. T. Russell, and M. Aubry, Satellite studies of magnetospheric substorms on August 15, 1968, 9, Phenomenological model for substorms, *J. Geophys. Res., 78*, 3131, 1973.

Mitchell, R. L., D. J. Williams, C. Y. Huang, L. A. Frank, and C. T. Russell, Current carriers in the near-earth cross tail current sheet during substorm growth phase, *Geophys. Res. Lett., 17*, 583, 1990.

Nagai, T., Observed magnetic substorm signatures at synchronous altitude, *J. Geophys. Res., 87*, 4405, 1984.

Nishida, A., and N. Nagayama, Synoptic survey for the neutral line in the magnetotail during the substorm expansion phase, *J. Geophys. Res., 78*, 3782, 1973.

Ogino, T., A three dimensional MHD simulation of the interaction of the solar wind with the earth's magnetosphere: The generation of field aligned currents, *J. Geophys. Res.*, 91, 6791, 1986.

Ogino, T., R. J. Walker and M. Ashour-Abdalla, Magnetic flux ropes in 3-dimensional MHD simulations, in *Physics of Magnetic Flux Ropes*, edited by C. T. Russell, E. R. Priest, and L. C. Lee, *Geophys. Monogr. Ser.*, vol. 58, p. 669, AGU, Washington, D.C., 1990*a*.

Ogino, T., R. J. Walker, and M. Ashour-Abdalla, Using global magnetohydrodynamic simulations to map phenomena from the magnetosphere to the polar ionosphere, (abstract), *EOS Trans. AGU, 71*, 604, 1990*b*.

Ogino, T., R. J. Walker, and M. Ashour-Abdalla, A global magnetohydrodynamic simulation of the magnetosheath and the magnetosphere when the interplanetary magnetic field is northward, *IEEE Trans. Plasma Sci., 70*, 487, 1992.

Pytte, T., R. L. McPherron, E. W. Hones, Jr., and H. I. West, Jr., Multiple satellite studies of magnetospheric substorms: Distinction between polar magnetic substorms and convection- driven negative bays, *J. Geophys. Res., 83*, 663, 1978.

Rostoker, G., and T. Eastman, A boundary layer model for magnetospheric substorms, *J. Geophys. Res., 92*, 12187, 1987.

Russell, C. T., and R. L. McPherron, The magnetotail and substorms, *Space Sci. Rev., 11*(111), 1973.

Schindler, K., A theory of the substorm mechanism, *J. Geophys. Res., 79*, 2803, 1974.

Schindler, K., and J. Birn, Self-consistent theory of time-dependent convection in the earth's magnetotail, *J. Geophys. Res., 87*, 2263, 1982.

Sergeev, V. A., and W. Lennartsson, Plasma sheet at $x = -20R_E$ during steady magnetospheric convection, *Planet. Space Sci., 36*, 353, 1988.

Sergeev, V. A., P. Tanskanen, K. Mursula, A. Korth, and R. C. Elphic, Current sheet thickness in the near-earth plasma sheet during substorm growth phase, *J. Geophys. Res., 85*, 3819, 1990.

Sheppard, G. G., and J. S. Murphree, Diagnosis of auroral dynamics using global auroral imaging with emphasis on localized and transient features, in *Auroral Physics*, edited by C.-I. Meng, M. J. Rycroft, and L. A. Frank, p.289, Cambridge University Press, New York, 1991.

Slavin, J. A., E. J. Smith, B. T. Tsurutani, D. G. Sibeck, H. J. Singer, D. N. Baker, J. T. Gosling, E. W. Hones, and F. L. Scarf, Substorm associated traveling compression regions in the distant tail: ISEE-3 geotail observations, *Geophys. Res. Lett., 11*, 7, 657, 1984.

Slavin, J. A., M. F. Smith, E. L. Mazur, D. N. Baker, T. Iyemori, H.J. Singer and E.W. Greenstadt, ISEE-3 plasmoid and TCR observations during an extended interval of substorm acitivty, *Geophys. Res. Lett., 19*, 825, 1992.

Smith, R. A., C. K. Goertz, and W. Grossman, Thermal catastrophe in the plasma sheet boundary layer, *J. Geophys. Res., 91*, 13, 1380, 1986.

Takahashi, K., L. J. Zanetti, R. E. Lopez, R. W. McEntire, T. A. Potemra, and K. Tumoto, Description of the magnetotail current sheet observed by AMPTE/CCE, *Geophys. Res. Lett., 14*, 1079, 1987.

Walker, R. J., T. Ogino and M. Ashour-Abdalla, A global magnetohydrodynamic model of magnetospheric substorms, in *Physics of Space Plasmas*, edited by T. Chang, G. B. Chew, and J. R. Jasperse, *Sci. Publ. Inc. Conf. Proc. Reprint Ser.*, vol. 7, 235, 1988.

Watanabe, K., and T. Sato, Global simulation of the solar wind-magnetosphere interaction: The importance of its numerical validity, *J. Geophys. Res., 95*, 75, 1990.

Wu, C. C., R. J. Walker, and J. M. Dawson, A three dimensional MHD model of the earth's magnetosphere, *Geophys. Res. Lett., 8*, 523, 1981.

M. Ashour-Abdalla, J. Raeder, and R. J. Walker, Institute of Geophysics and Planetary Physics, University of California Los Angeles, 405 Hilgard Avenue, Los Angeles, CA 90024-1567.

T. Ogino, Solar Terrestrial Environment Laoratory, Nagoya University, Toyokawa Aichi, 442 Japan.

(Received June 18, 1992;
revised April 27, 1993;
accepted April 30, 1993.)